The astrochemical factory: A solid base for interstellar reactions

Ligterink, N.F.W.

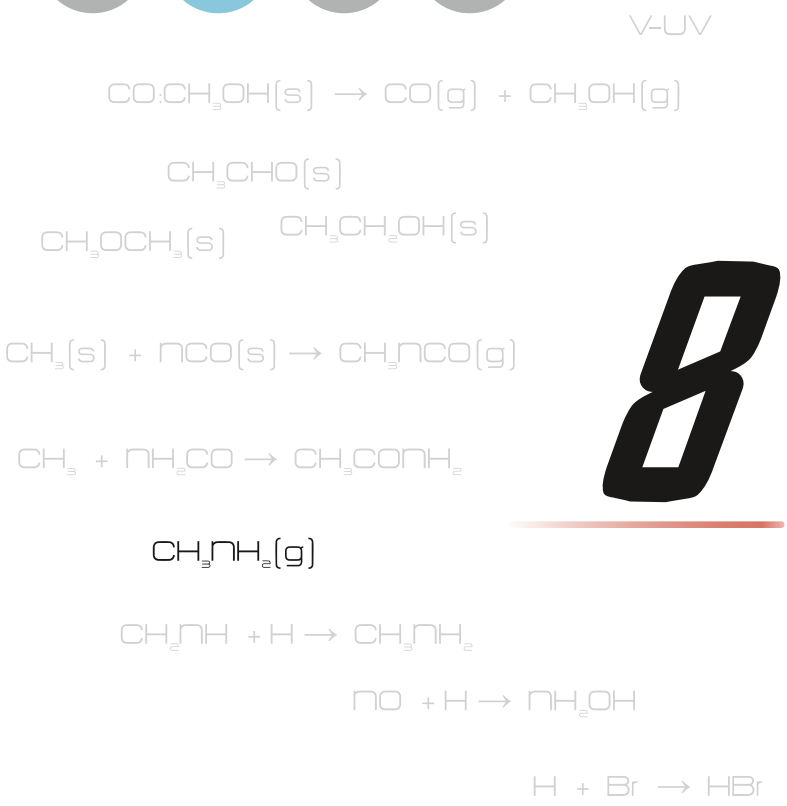

8

Search for methylamine in high mass hot cores

N.F.W. Ligterink, E.D. Tenenbaum & E.F. van Dishoeck

Ligterink et al. 2015a, *Search for methylamine in high mass hot cores*, A&A 576, A35

8.1. Introduction

Complex organic molecules are thought to be formed primarily on dust grains in dense cores, see reviews by Herbst & van Dishoeck (2009) and Caselli & Ceccarelli (2012). Before the onset of star formation, the atomic and molecular reservoir is contained in large dark clouds. Due to the high densities ($\geq 10^4$ cm^{-3}) and low temperatures (10 K) reached in these environments, gas-phase species will freeze out on sub-micron sized grains forming ice mantles on timescales shorter than the lifetime of the cloud. It is here that atoms and molecules can potentially react with each other to form the zeroth order ice species like ammonia, methane, water and methanol. UV radiation interacts with these ice mantles by dissociating molecules to produce radicals and by photodesorbing species back to the gas phase. If these radicals are sufficiently mobile, they can find each other on the grain and react to form even more complex first generation (organic) species (Garrod & Herbst 2006). However, it is not entirely clear if UV radiation is essential to form these complex molecules or whether they can also be formed just by thermal processing and atom bombardment of solid CO with C, N and O atoms (Tielens & Charnley 1997).

In this context methylamine, CH_3NH_2, is a particularly interesting molecule, since its formation is hypothesised by Garrod et al. (2008) to be completely dependent on radicals produced by UV photons, and is one of the few molecules that can definitely not be produced in the routes starting from solid CO:

$$CH_4 + h\nu \rightarrow CH_3^\bullet + H \tag{8.1}$$

$$NH_3 + h\nu \rightarrow NH_2^\bullet + H \tag{8.2}$$

$$CH_3^\bullet + NH_2^\bullet \rightarrow CH_3NH_2 \tag{8.3}$$

These radicals can form in the ice mantles in the dark cloud or in the protostellar phase through cosmic-ray induced photons and/or UV photons from the protostar. After gravitational collapse of the cloud and formation of a protostar, the dust around it will start to warm up. The increased temperature will cause the radicals to become mobile on the grains and react with each other, forming methylamine. Further heating will evaporate the formed methylamine from the grain and raise its gas-phase abundance.

Another interesting amine-containing molecule is formamide, NH_2CHO. This is so far the most abundantly observed amine-containing molecule (e.g., Bisschop et al. 2007b; Halfen et al. 2011), making it an interesting molecule to compare with other amines like methylamine. In contrast with CH_3NH_2, this molecule can possibly be produced by reactions of H and N with solid CO. The comparison of the abundances of these two species could potentially give more information about the relative importance of UV-induced versus thermal grain surface reactions.

Hot cores are particularly well-suited to study methylamine. These high mass star-forming regions reach high temperatures between 100 to 300 K and are known for their rich complex organic chemistry (Walmsley 1992; van Dishoeck & Blake 1998; Tielens & Charnley 1997; Ehrenfreund & Charnley 2000; Caselli &

Ceccarelli 2012). The ice covered grains move inwards to the protostar and will heat up. When sufficient temperatures are reached, molecules will start to desorb depending on their respective binding energies. Less abundant molecules mixed with water ice will desorb together with water around 100 K.

Previous detections of methylamine have all been made toward the galactic center. Kaifu et al. (1974) first detected CH_3NH_2 in Sagittarius B2 and Orion A. Later that same year Fourikis et al. (1974) reported the detection of methylamine in the same sources, but with a different telescope. Much more sensitive surveys by Turner (1991), Nummelin et al. (2000), Halfen et al. (2013), Belloche et al. (2013) and Neill et al. (2014) also all detected methylamine lines toward SgrB2, with typical inferred abundance ratios with respect to NH_2CHO between 0.5 to 3. No detections of methylamine have been reported in sensitive surveys with modern detectors toward Orion, however (Blake et al. 1987; Turner 1991; Sutton et al. 1995; Schilke et al. 1997; Crockett et al. 2014b).

To study the importance of UV processing of ice-covered dust grains, we present the results of searches for methylamine in a number of hot cores (see Table 8.1). These results are combined and compared with data from Bisschop et al. (2007b) and Isokoski et al. (2013), which were taken toward the same hot cores with the same telescope and analysis method and include detections of NH_2CHO and other nitrogen-containing species. In Section 8.2 the observational details are given, followed by the analysis method in Section 8.3. Section 8.4 summarizes all the results of our analysis and these are discussed in Section 8.5. Finally conclusions are drawn in Section 8.6.

8.2. Observations

Observations were performed with the James Clerk Maxwell Telescope (JCMT) [1] on the sources listed in Table 8.1 between July 2010 and August 2011. The sources were selected based on their particularly rich chemistry, being isolated, having narrow line widths to prevent line confusion and on their relatively nearby distance (Bisschop et al. 2007b; Fontani et al. 2007; Rathborne et al. 2008; Isokoski et al. 2013).

Nummelin et al. (1998) detected methylamine emission lines between 218 to 263 GHz toward Sgr B2N. Therefore the RxA3 front-end double side band receiver, functioning between 210 to 276 GHz, was chosen to observe the hot cores. The 250 and 1000 MHz wide back-end ACSIS configurations were used. A number of methylamine transitions covering a range of excitation energies were selected in this frequency range based on high Einstein A coefficients and lack of line confusion (Table 8.2). However, not all transitions were observed for all sources. The 235735 MHz transition was only recorded for W3(H_2O) and the 260293 MHz transition only toward W3(H_2O) and NGC 7538 IRS1.

Because double side band spectra were obtained, our spectra contain transitions from two different frequency regimes superposed. To disentangle lines from the two side bands, each source was observed twice with an 8 MHz

[1]The James Clerk Maxwell Telescope is operated by the Joint Astronomy Centre on behalf of the Science and Technology Facilities Council of the United Kingdom, the National Research Council of Canada, and (until 31 March 2013) the Netherlands Organisation for Scientific Research.

Table 8.1: Source list and source parameters

Source	RA J2000	Dec J2000	θ_S^a AU	θ_B^a AU	L^a $L_\odot$	d^a (kpc)	V_{LSR} (km s^{-1})	ΔV (km s^{-1})	$\delta\nu$ (km s^{-1})	RMS (mK)
AFGL 2591	20:29:24.60	+40:11:18.9	1800	21000	2.0E+05	3.3	-5.5	4.0	1.28	10
G24.78	18:36:12.60	−07:12:11.0	13000	162000	7.9E+05	7.7	111.0	6.3	1.28	9
G31.41+0.31	18:47:34.33	−01:12:46.5	7840	166000	2.6E+05	7.9	98.7	7.3	1.28	7
G75.78	20:21:44.10	+37:26:40.0	5600	86100	1.9E+05	4.1	-0.04	5.6	1.28	9
IRAS 18089-1732	18:11:51.40	−17:31:28.5	2750	49000	3.2E+04	2.3	33.8	4.5	1.28	9
IRAS 20126+4104	20:14:26.40	+41:13:32.5	1753	34400	1.3E+04	1.6	-3.8	6.0	1.28	10
NGC 7538 IRS1	23:13:45.40	+61:28:12.0	4900	58800	1.3E+05	2.8	-57.4	4.0	1.28	10
W3(H_2O)	02:27:04.60	+61:52:26.0	2400	42000	2.0E+04	2.0	-46.4	5.0	1.28	11
W 33A	18:14:38.90	−17:52:04.0	4500	84000	1.0E+05	4.0	37.5	4.9	1.28	11

Notes. [a]Data for AFGL 2591 taken from (Rygl et al. 2012). Other data taken from Bisschop et al. (2007b) and Isokoski et al. (2013).

Table 8.2: Methylamine transitions observed in this study[a]

Transition	Freq (MHz)	E_{up} (K)	A (s^{-1})	g_{up}
$4_2 \rightarrow 4_1$ [b]	229310.298	36.9	1.32E-05	108
$7_2 \rightarrow 7_1$ [b]	229452.603	75.5	5.88E-06	60
$8_2 \rightarrow 8_1$ [c]	235735.037	92.8	6.13E-05	204
$6_2 \rightarrow 6_1$ [b]	236408.788	60.8	5.94E-05	52
$2_2 \rightarrow 2_1$ [b]	237143.530	22.0	3.82E-05	60
$10_2 \rightarrow 10_1$ [d]	260293.536	132.7	2.26E-05	52

Notes. [a] Data from JPL database for molecular spectroscopy. [b] Transition observed in all sources. [c] Only observed in W3(H_2O). [d] Only observed in W3(H_2O) and NGC 7538 IRS1.

shift in the local oscillator setting between the two observations. This allows each transition to be uniquely assigned to either of the two side bands.

In the 230 GHz band, the JCMT has a beam size (θ_B) of 20-21″. Spectra were scaled from the antenna temperature scale, T_A^*, to main beam temperature, T_{MB}, by using the main beam efficiency of 0.69 at 230 GHz. Integration times were such that T_{RMS} is generally better than 10 mK for data binned to 1.3 km s^{-1} velocity bins. Noise levels were improved by adding the shifted spectra together in a narrow frequency region around the CH_3NH_2 lines, effectively doubling the integration time.

8.3. Data analysis

To analyse the data, exactly the same method as described by Bisschop et al. (2007b) and Isokoski et al. (2013) was used. It will be shortly reiterated here. The hot core spectra corrected for source velocity were analysed with the "Weeds" extension (Maret et al. 2011) of the Continuum and Line Analysis Single-dish Software (CLASS[2]) coupled with the Jet Propulsion Laboratory (JPL[3]) database for molecular spectroscopy (Pickett et al. 1998). Focus was on identifying the transitions of methylamine listed in Table 8.2, but other lines in the spectra were measured as well (see Table 8.5 Appendix). After each positive identification the integrated main-beam temperature, $\int T_{MB} dV$, was determined by gaussian fitting of the line. From the integrated main-beam intensity the column density N_{up} and thus the *beam*-averaged total column density N_T could be determined, assuming Local Thermodynamic Equilibrium (LTE) at a single excitation temperature T_{rot}:

$$\frac{3k \int T_{MB} dV}{8\pi^3 \nu \mu^2 S} = \frac{N_{up}}{g_{up}} = \frac{N_T}{Q(T_{rot})} e^{-E_{up}/T_{rot}} \tag{8.4}$$

where g_{up} is the level degeneracy, k the Boltzmann constant, ν the transition

[2] **http://www.iram.fr/IRAMFR/GILDAS**
[3] **http://spec.jpl.nasa.gov**

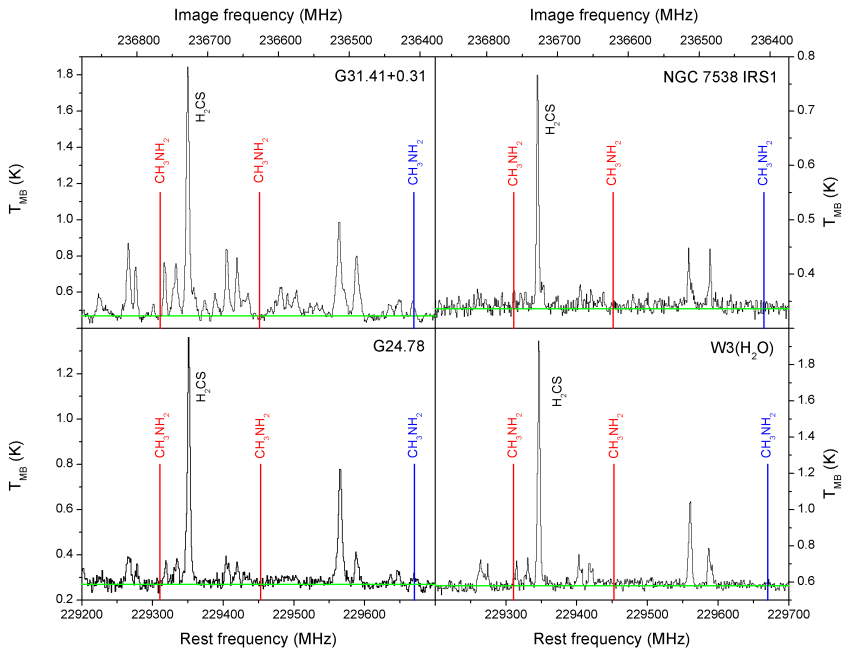

Figure 8.1: JCMT spectra of the massive hot cores G31.41+0.31, G24.75, NGC 7538 IRS1 and W3(H_2O). The 229310 and 229452 MHz transitions in the lower sideband are indicated in red and that at 236408 MHz in the upper sideband in blue. In green is the baseline, obtained by fitting line free portions of the spectrum. In all spectra the H_2CS $7_1 \rightarrow 6_1$ transition at 236726 MHz is fitted to determine the typical linewidth in the sources, as listed in Table 8.1.

frequency, μ the dipole moment and S the line strength. $Q(T_{\rm rot})$ is the rotational partition function and $E_{\rm up}$ is the upper state energy in Kelvin.

In case of a non-detection, 3σ upper limits were determined from the Root Mean Square (RMS) of the base line of the spectra in combination with the velocity resolution $\delta\nu$ and line width ΔV:

$$\text{œ} = 1.2\sqrt{\delta\nu\Delta V}\cdot \text{RMS} \tag{8.5}$$

ΔV is estimated from other transitions (see Table 8.1) in the spectra, for example from the nearby H_2CS $7_1 \rightarrow 6_1$ transition, and assumed to be the same for all transitions in the spectral range. A telescope flux calibration error of 20% is taken into account in the 1.2 factor. The 3σ value is then used in the same way as the main-beam intensity of detected lines to obtain the upper limit on the total column density through Eq. 8.4.

Since no rotational temperature can be determined for a non-detection, this has to be estimated. In the models of Garrod et al. (2008) the peak abundance temperatures for methylamine range from 117 to 124 K depending on the model used. Öberg (2009) determined that methylamine forms in CH_4/NH_3 UV irradiation experiments and sublimates at 120 K. There is a small difference between laboratory and hot core desorption temperatures, because

of the pressure difference between the two. Also, if CH_3NH_2 is embedded in water ice the desorption temperature will probably be limited to roughly 100 K, when water desorbs in space. Therefore $T_{\rm rot}$ is assumed to be 120 K when methylamine lines could not be identified, but the effects of lower and higher rotation temperatures are explored as well.

Correction for beam dilution is done in the same way as Bisschop et al. (2007b):

$$\eta_{BF} = \frac{\theta_S^2}{\theta_S^2 + \theta_B^2} \tag{8.6}$$

resulting in the *source*-averaged column density:

$$N_S = \frac{N_T}{\eta_{BF}} \tag{8.7}$$

The beam diameter θ_B is set at 21″. For the source diameter, θ_S, values have been taken from Bisschop et al. (2007b) and Isokoski et al. (2013) and constitute the area where the temperature is 100 K or higher and hot gas-phase molecules are present. Both beam and source diameters are listed in AU in Table 8.1. Using the CASSIS line analysis software [4] it was verified that the source-averaged column densities are still small enough that the observed lines are optically thin.

8.4. Results

8.4.1. CH_3NH_2 limits

Figure 8.1 presents examples of spectra obtained for our sources, whereas Figure 8.4 in the Appendix shows the $2_2 - 2_1$ line in all sources. In general, no transitions of CH_3NH_2 are detected. Only one possible methylamine transition is identified in G31.41+0.31 coincident with the $6_2 \rightarrow 6_1$ line at 236408 MHz, with an integrated intensity of 0.44 K kms^{-1}. Following the procedure summarized in Section 8.3, a column density of 3.4×10^{17} cm^{-2} is inferred from this line assuming $T_{\rm rot} = 120$ K. However, modelling of the spectrum shows that the other targeted CH_3NH_2 lines, $4_2 \rightarrow 4_1$ and $2_2 \rightarrow 2_1$, should have comparable or even higher intensities if this identification is correct (Figure 8.3). The $8_2 \rightarrow 8_1$ line should be readily detected but was not observed toward G31.41+0.31. This makes it unlikely that the detected feature belongs to methylamine, since we would expect to see at least two other CH_3NH_2 transitions in our spectrum.

In Figure 8.2 upper limit column densities of the six investigated transitions of methylamine are plotted versus rotational temperature taking a typical 3σ = 0.100 K kms^{-1}. At 120 K the $8_2 \rightarrow 8_1$, 235735 MHz transition gives the lowest limits on the column densities, see Figure 8.2. However, since this particular transition was only included in the observations for one source, the second most sensitive transition at 120 K, $2_2 \rightarrow 2_1$, will be used (see Figure 8.4 in the Appendix for a blow-up of this particular spectral region in all investigated sources). All

[4] CASSIS has been developed by IRAP-UPS/CNRS (http://cassis.irap.omp.eu).

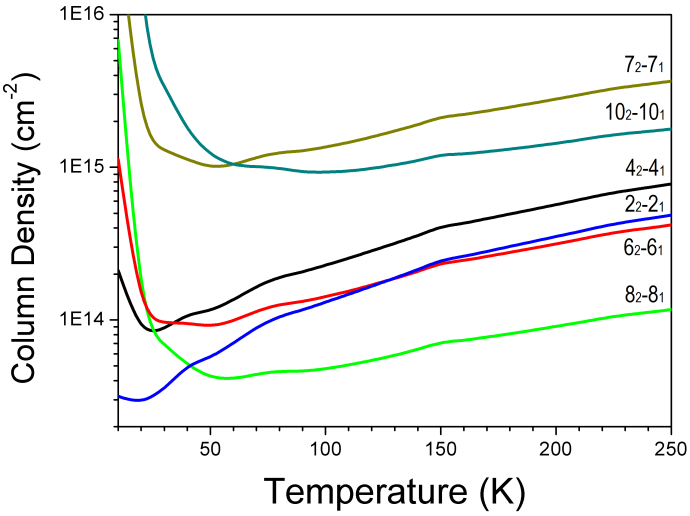

Figure 8.2: Column densities for the six methylamine transitions plotted versus temperature. This plot is made for a 3σ limit of 0.1 K kms^{-1}, as found for W3(H_2O). This figure demonstrates that the $8_2 - 8_1$ transition (green) gives the most sensitive limits on column density for the relevant range of excitation temperatures in hot cores, when observed. The other five transitions ($4_2 \rightarrow 4_1$, black; $7_2 \rightarrow 7_1$, gold; $10_2 \rightarrow 10_1$, cyan; $2_2 \rightarrow 2_1$, blue and $6_2 \rightarrow 6_1$, red) clearly imply higher column densities. Only below 40 K does the $2_2 \rightarrow 2_1$ line give lower column density limits.

following molecular ratios are based on CH_3NH_2 column densities obtained from this line, assuming T_{rot} = 120 K. The corresponding upper limits are presented in Table 8.3

8.4.2. Abundance ratio comparison

Combined with NH_2CHO and CH_3OH column densities from Bisschop et al. (2007b) and Isokoski et al. (2013) derived in the same way, abundance ratios for methylamine and formamide with respect to each other and to methanol are calculated. These ratios are listed in Table 8.3. Methanol is chosen as a reference since it is the most readily observed complex organic molecule. Its disadvantage is that some of the transitions have high optical depth and that a cold component may be present (Isokoski et al. 2013), but this is circumvented by only taking the warm methanol column density derived from optically thin lines. Abundances relative to methanol rather than H_2 are preferred since the H_2 column depends on extrapolation of dust models to smaller scales than actually observed (Bisschop et al. 2007b). Another point that needs to be taken into account is that the models of Garrod et al. (2008) do show a slight overproduction of CH_3OH, which could influence the comparison between the ratios. Overall, the abundance ratios are estimated to be accurate to a factor of a few.

It should be noted that methylamine and formamide have significantly different dipole moments (1.31 and 3.73 Debye respectively) and could therefore

be excited in different ways. Formamide has a larger critical density than methylamine, so the situation could arise where the critical density is not reached for formamide or even both molecules. The corresponding excitation temperatures will then be lower. In particular, the situation in which the critical density is not reached for formamide but is for methylamine, could affect the inferred ratios. As can be seen from Figure 8.2, if $T_{\rm rot}$ drops from 120 to 50 K, the column density drops by a factor of a few, depending on transition. If $T_{\rm rot}$ were 120 K for methylamine but 50 K for formamide, the observed column density of formamide would be lower than that listed here and thus result in a higher CH_3NH_2/NH_2CHO ratio. We note, however, that there is no observational evidence that $T_{\rm rot}$ is systematically lower than 100 K for formamide (Bisschop et al. 2007b).

Table 8.3 includes the observational results toward Sgr B2, the only source where methylamine is firmly detected, from Turner (1991), Belloche et al. (2013) and Neill et al. (2014). These results, obtained over the course of more than two decades, agree well with each other within the estimated uncertainties due to slightly different adopted source sizes. Nummelin et al. (2000) also detect methylamine in their Sgr B2 survey but find a surprisingly small beam filling factor and consequently very large column density compared with most other complex organic molecules. If their beam filling factor for CH_3NH_2 is taken to be the same as for NH_2CHO, the Nummelin et al. (2000) ratios are more in line with those derived by Turner (1991), Belloche et al. (2013) and Neill et al. (2014). The non-detections of methylamine toward the chemically rich and well studied Orion hot core imply abundance limits that are at least a factor of 5 lower than for SgrB2 (Neill et al. 2014; Crockett et al. 2014b).

Table 8.3 also contains the model results from Garrod et al. (2008), who present three hot core models which differ from each other by their warm-up timescale from 10 to 200 K. The timescales for F(ast), M(edium) and S(low) are 5×10^4, 2×10^5 and 1×10^6 years, respectively, and start after the cold collapse phase. In the slow models more time is spent in the warm-up phase where radicals are mobile. Values used in this comparison are taken from the so-called reduced ice composition, where cold phase methane and methanol abundances were modified to match observations of these ices toward W33A, NGC 7538 IRS9 and Sgr A*, see Gibb et al. (2000b). Another comparison can be made with the gas-phase abundances in protoplanetary disk models of Walsh et al. (2014) which have similar or higher densities and temperatures as in protostellar cores. Their ratios range from 7.2×10^{-1} to 6.5×10^{-2} for CH_3NH_2/CH_3OH, 4.2×10^{-1} to 1.5 for CH_3NH_2/NH_2CHO and 1.7 to 8.8×10^{-2} for the NH_2CHO/CH_3OH. These ratios are close to the predicted values of Garrod et al. (2008) listed in Table 8.3, which may be partly due to using the same surface-chemistry network.

From Table 8.3 several trends become apparent for our results. The CH_3NH_2/NH_2CHO limits lie about an order of magnitude above model values whereas the CH_3NH_2/CH_3OH limit approximately matches with theoretical predictions. Because the observed values are actually 3σ upper limits, this suggests that models overproduce CH_3NH_2. For the sources with the most stringent limits, such as G31.41+0.31 and the $8_2 - 8_1$ line in W3(H_2O), the CH_3NH_2/CH_3OH limits are comparable or even lower than the abundance ratios for Sgr B2. The third ratio, NH_2CHO/CH_3OH, is also found to be lower than the

models by up to one order of magnitude.

Close inspection of the Bisschop et al. (2007b) data shows that the NH_2CHO column densities may have larger uncertainties than quoted in their figures and tables. We have therefore re-analysed all NH_2CHO data from that paper taking larger uncertainties into account. In general, this leads to lower NH_2CHO column densities. Even using the upper limits from this re-analysis as well as those from Isokoski et al. (2013) (which were obtained with generous error bars), the NH_2CHO_{upper}/CH_3OH ratios are significantly lower than the models. This suggests that both the methylamine and formamide abundances are too high in the models.

The Sgr B2 detections tend to have lower CH_3NH_2/NH_2CHO and CH_3NH_2/CH_3OH ratios than our upper limits and are also somewhat below the models, but generally do not differ more than a factor of a few. The SgrB2 NH_2CHO/CH_3OH ratios are also closer to the models results, at least for the faster models. However, the Orion Compact Ridge NH_2CHO/CH_3OH value from Crockett et al. (2014b) is comparable to that found for our sources and clearly lower than the models. Further observations are needed to determine to what extent Sgr B2 is a special case.

To further elucidate the differences between theory and our and the Sgr B2 observations, an additional analysis was made of the CH_3NH_2/CH_3CN ratio. These results are listed in Table 8.4. Acetonitrile is produced in the gas-phase, but more abundantly on grains: an important route to its formation is via $CH_3^\bullet$ + $CN^\bullet \rightarrow CH_3CN$, according to Garrod et al. (2008). This would mean that both molecules compete for the methyl radical on the surface, thus relating the two molecules.

Our observed ratios involving CH_3CN are clearly at odds with the theoretical predictions. The observed CH_3NH_2/CH_3CN ratios are in most cases an order of magnitude lower than theory and approach the observed ratios for Sgr B2. However, the observed CH_3CN/CH_3OH ratios are 1-2 orders of magnitude higher than theoretical predictions. Both these cases point to CH_3CN being underproduced in the models.

Finally, abundance ratios, with some notable exceptions, do not vary more than an order of magnitude between different sources, as also found by Bisschop et al. (2007b) for other species.

8.5. Discussion

Despite a significant number of succesfully identified molecules (see Table 8.5 in the Appendix for examples of W3(H_2O) and G31.41+0.31), only upper limits were found for methylamine in the various hot cores, limiting the conclusions that can be drawn. Nevertheless, trends are seen in our abundance ratios. The results suggest that theoretically predicted abundances for both methylamine and formamide are too high. In contrast, acetonitrile is found to be underproduced in the models. In the following, each of these species is discussed individually.

Table 8.3: Upper limit column densities and abundance ratios for methylamine.

Source	N_{S,CH_3NH_2} cm^{-2}	CH_3NH_2/NH_2CHO	CH_3NH_2/CH_3OH	NH_2CHO/CH_3OH	NH_2CHO_{upper}/CH_3OH
Model F		1.1	3.4E-02	3.1E-02	3.1E-02
Model M		1.7	1.0E-01	7.3E-02	7.3E-02
Model S		1.3	1.3E-01	1.0E-01	1.0E-01
AFGL 2591	≤1.9E+16	-	-	≤3.9E-01	-
G24.78	≤2.4E+16	≤3.3E+01	≤8.5E-02	2.6E-03	9.0E-04
G31.41+0.31	≤5.8E+16	≤2.8E+01	≤4.9E-02	1.8E-03	3.8E-03
G75.78	≤3.5E+16	≤1.7E+02	≤3.1E-01	1.8E-03	2.6E-02
IRAS 18089-1732	≤4.2E+16	≤5.0E+01	≤1.9E-01	3.8E-03	7.9E-03
IRAS 20126+4104	≤6.4E+16	-	≤2.2	-	-
NGC 7538 IRS1	≤2.0E+16	≤3.5E+01	≤1.8E-01	4.8E-03	2.1E-04
W3(H_2O)	≤5.0E+16	≤3.9E+01	≤5.0E-02	1.3E-03	6.4E-04
W3(H_2O)*	≤1.7E+16	≤1.3E+01	≤1.7E-02	1.3E-03	6.4E-04
W 33A	≤5.7E+16	≤2.7E+01	≤2.9E-01	1.1E-02	4.6E-03
Sgr B2[a]	1.2E+14	5.7E-01	1.7E-02	1.3E-02	
Sgr B2(M)[b]	4.5E+16	3.2	1.7E-02	5.2E-03	
Sgr B2(N)[b]	6.0E+17	4.3E-01	3.3E-02	7.8E-02	
Sgr B2(N)[c]	5.0E+17	2.1	1.0E-01	4.8E-02	
Orion Compact Ridge[d]	-	-	-	1.6E-03	

Notes. Column densities for the assumed source size and upper limit abundance ratios for methylamine, derived from the $2_2 - 2_1$ line assuming T_{rot} = 120 K. The values for NH_2CHO and CH_3OH where taken from Bisschop et al. (2007b) and Isokoski et al. (2013). The upper limits of NH_2CHO were determined by our own re-analysis of the Bisschop et al. (2007b) data and taken from the appendix of Isokoski et al. (2013). * Column density calculated for the $8_2 - 8_1$ line. **References.** [a] Turner (1991), beam sizes between 65″ and 107″, assuming no beam dilution; [b] Belloche et al. (2013), beam sizes between ∼25″ and ∼30″, assuming a 3″ source size for (N) and 5″ source size for (M); [c] Neill et al. (2014), beam sizes between ∼10″ and ∼40″, assuming source size of 2.5″; and [d]Crockett et al. (2014b) beam sizes between 44″ and 11″ and assuming a 10″ size of the Compact Ridge.

Table 8.4: Upper limit column densities and abundance ratios for methylamine.

Source	CH_3NH_2/CH_3CN	CH_3CN/CH_3OH
Model F	5.5E+01	6.3E-04
Model M	3.8E+01	2.6E-03
Model S	1.5E+01	8.6E-03
AFGL 2591	$\leq$5.3	$\leq$7.5E-02
G24.78	$\leq$5.1E-01	2.1E-01
G31.41+0.31	$\leq$3.6	5.9E-02*
G75.78	$\leq$1.9E+01	1.6E-02
IRAS 18089-1732	$\leq$8.9	1.1E-02*
IRAS 20126+4104	$\leq$4.3E+01	5.2E-02
NGC 7538 IRS1	$\leq$2.5	6.8E-02
W3(H_2O)	$\leq$7.2	7.0E-03
W 33A	$\leq$2.1	1.4E-01
Sgr B2[a]	1.2	1.5E-02
Sgr B2(N)[b]	3.0E-01	1.1E-01
Sgr B2(M)[b]	2.5E-01	6.7E-02
Sgr B2(N)[c]	5.9E+01	1.7E-02
Orion Compact Ridge[d]	-	1.1E-02

Notes. Abundance ratios for methylamine. The values for CH_3OH and CH_3CN were taken from Bisschop et al. (2007b) and Isokoski et al. (2013). *Ratio derived from optically thin ^{13}C isotope. [a] Turner (1991), [b] Belloche et al. (2013), [c] Neill et al. (2014) and [d] Crockett et al. (2014b).

8.5.1. CH_3NH_2

Garrod et al. (2008) suggest that methylamine is primarily formed by grain-surface chemistry using UV to create the CH_3 and NH_2 radicals from photodissociation of primarily CH_4 and NH_3. Perhaps the amount of UV processing is overestimated in these models. An alternative route is hydrogen atom addition to solid HCN, proposed by Theule et al. (2011) and found to lead to both CH_2NH (methanimine) and CH_3NH_2. Walsh et al. (2014) find in their models that methylamine is indeed efficiently formed on grains at 10 K by atom addition reactions to solid CH_2NH. Burgdorf et al. (2010) have detected HCN ice on Triton, but so far no detection of solid HCN has been made in the ISM. Methanimine is actually readily observed in the gas-phase (Turner 1991; Nummelin et al. 1998; Belloche et al. 2013) so the presence of both species makes the H-atom addition scheme probable. However, Halfen et al. (2013) detect CH_2NH in Sgr B2(N) at a rotational temperature of 44 K, which is distinctly colder than the 159 K observed for CH_3NH_2, suggesting that the two molecules may not co-exist. An alternative route would therefore be to form these molecules by two different gas-phase reaction pathways ($CH^{\bullet}(g) + NH_3(g) \rightarrow CH_2NH + H$ and $CH_3^{\bullet}(g) + NH_3(g) \rightarrow CH_3NH_2 + H$), with CH being present primarily in the colder outer envelope and CH_3 in the warmer center. Further modeling is needed to determine whether these gas-phase reactions can reproduce the

observed abundances quantitatively.

8.5.2. NH_2CHO

Formamide also appears to be overproduced in the hot core model. Since Garrod et al. (2008) use both gas-phase, radical and atom addition reactions to form formamide, it is difficult to pin down where the discrepancies could come from. It is known that NH_2CHO is formed in CO:NH_3 mixtures after UV and electron irradiation (Grim et al. 1989; Demyk et al. 1998; Jones et al. 2011) and it has also been proposed that it can form from H- and N-atom addition to solid CO (Tielens & Charnley 1997). Gas-phase formation from CO and NH_3 is viable as well (Hubbard et al. 1975), although these experiments were conducted under high-pressure conditions, not the low pressures applicable in the ISM. Further quantification of both gas-phase and solid phase routes through laboratory experiments is needed. Recent laboratory experiments by Fedoseev et al. (2015b) do not find NH_2CHO production in H- and N-atom bombardment studies of solid CO, consistent with a large barrier for H- addition to HNCO found in ab initio calculations (Nguyen et al. 1996), so perhaps the efficiency of this route has been overestimated in the models. An alternative solution would be that the high-mass sources studied here have not gone through a long (pre-stellar) phase in which the dust temperature was low enough for CO to be frozen out and turned into other molecules.

8.5.3. CH_3CN

The clear mismatches between theory and observations for the ratios involving CH_3CN point toward an underproduction of acetonitrile by more than an order of magnitude in the models. As with formamide, gas-phase, radical and atom addition reactions contribute to the formation of CH_3CN in the models, making it difficult to determine the cause. The main formation route in the models by radical addition of solid $CH_3^\bullet$ and solid $CN^\bullet$ has never experimentally been investigated. It would therefore be useful to determine if this is a viable solid state formation route and if it potentially has a higher efficiency than assumed.

Alternatively it is possible that photodestruction of solid acetonitrile is not as efficient as assumed in the models. Gratier et al. (2013) find high gas-phase CH_3CN abundances in the Horsehead PDR, indicative of a high photodesorption rate and slow destruction of CH_3CN in the ice. Bernstein et al. (2004) indeed find slower photolysis of solid CH_3CN compared with other organic molecules. If such a slower photodissociation rate would also hold for gas-phase CH_3CN, it would be an attractive explanation why the CH_3CN rotational temperatures are generally higher than those of other complex molecules (e.g., Bisschop et al. (2007b) and many other hot core studies), since the molecule could then approach the protostar closer before being destroyed. However, the gas phase photoabsorption cross sections of CH_3CN are well determined and if the bulk of these absorptions lead to dissociation this would result in a photodissociation rate of gaseous CH_3CN at least as fast as that of CH_3OH (van Dishoeck et al. 2006).

Another important parameter for all molecules studied here is the mobility of radicals and neutral molecules on the surface assumed in the gas-grain models. For many species no experimental data are available on diffusion barriers, only theoretically-inspired guesses. Observational evidence suggests that at least parts of the ice mantles are segregated in CO-rich and CO-poor layers (Tielens et al. 1991; Pontoppidan et al. 2008). Therefore, more knowledge of the structure of ice mantles and the mobility of radicals and neutral molecules as a function of surface temperature and in various chemical environments is necessary to determine if addition reactions are likely to happen and at which rates.

8.5.4. Prospects for ALMA

In the near future, much deeper searches for CH_3NH_2 can be carried out by ALMA (Appendix 8.7.2). Figure 8.5 shows that the strongest transitions within Band 6 are mainly located between 240 and 275 GHz and in Band 7 around 310, 340 and 355 GHz. In Table 8.6 the strongest transitions in ALMA's Band 6 and 7 are listed. It becomes apparent that lines covered by Band 7 are more intense, but at the cost of a lower line density.

Estimates done for the W 33A source with the CASSIS line analysis software and the ALMA Sensitivity Calculator show that ALMA should be able to reach the 3σ detection limits for the CH_3NH_2 lines around 236 GHz in less than 1 hour of integration time, assuming the column density for methylamine of 1.2×10^{14} cm^{-2} as found by Turner (1991) in a large beam and two orders of magnitude lower than those inferred here for a small source size. This estimate assumes a spectral resolution of 0.64 kms^{-1} as used in our JCMT data, the number of ALMA antennas set to 34 (as in Cycle 2) and a synthesized beam of 1.1", appropriate for the W33A hot core (100 K radius).

8.6. Conclusions

We have analysed nine hot core regions in search of methylamine. The molecule has not been convincingly detected, so upper limit abundances are determined for all the sources. From these limits, ratios of methylamine to other molecules (NH_2CHO, CH_3OH, CH_3CN) have been determined and compared with theory and Sagittarius B2 surveys. Our conclusions are as follows:

1. Trends in our results indicate that both methylamine and formamide are overproduced in the models of Garrod et al. (2008). Acetonitrile is underproduced with respect to these models. This is especially true for the slow models.

2. Abundance ratios do not differ more than an order of magnitude between various sources suggesting that the (nitrogen) chemistry is very similar between hot cores, as has been found previously for other species.

3. More (laboratory) studies are needed to clarify the formation pathway of methylamine and to determine differences and similarities with formamide, methanimine and, to a lesser extent, acetonitrile formation.

4. The upper limits determined for CH_3NH_2 here can guide future more sensitive observations, especially with ALMA. Based on the ratios found in the Sgr B2 observations it is very likely that ALMA will reach the detection limit for methylamine in the sources studied here. Particularly strong transitions and spectral regions to target with ALMA are given.

Acknowledgement

Thanks go out to C. Walsh, I. San Jose García, M. Drozdovskaya, N. van der Marel, M. Kama, M. Persson, J. Mottram, G. Fedoseev, M.H.D. van der Wiel and H. Linnartz for their support and input on this project. Thoughtful comments by the referee are much appreciated.
Astrochemistry in Leiden is supported by the Netherlands Research School for Astronomy (NOVA), by a Royal Netherlands Academy of Arts and Sciences (KNAW) professor prize, and by the European Union A-ERC grant 291141 CHEMPLAN.

8.7. Appendix

8.7.1. Transitions of methylamine and other molecules

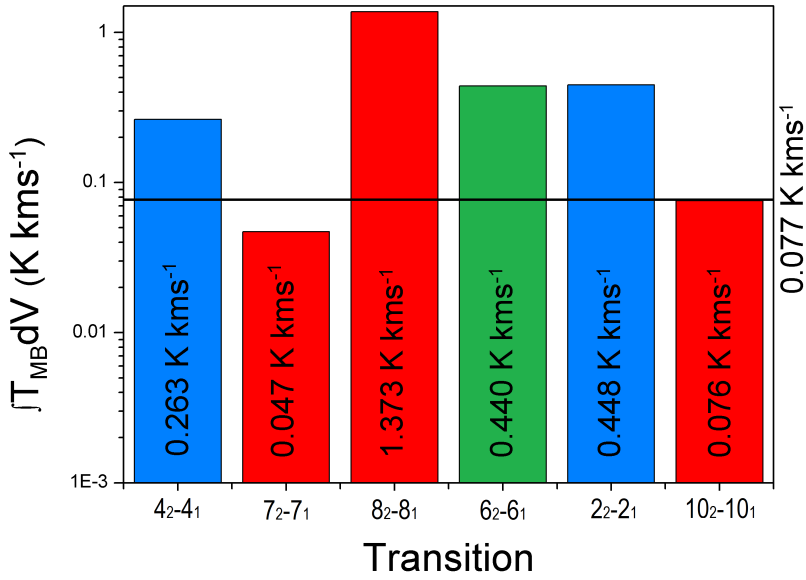

Figure 8.3: Bargraph plot of the integrated main-beam intensities for the six investigated methylamine transitions. $\int T_{\rm MB} dV$ values were calculated for a total column density of 3.4×10^{17} cm^{-2} as inferred toward G31.41+0.31 from the $6_2 \rightarrow 6_1$ transition, assuming a rotational temperature of 120 K. The horizontal line shows the 0.077 K kms^{-1} 3σ value for G31.41+0.31. It is unlikely that the detection of the 236408 feature (green) in this hot core is methylamine, since the main-beam intensities of other CH_3NH_2 transitions are above the 3σ value. Particularly the $4_2 \rightarrow 4_1$ and $2_2 \rightarrow 2_1$ transition (blue) should be visible in our spectra. The remaining transitions (red) are either below detection limit or not observed toward this source.

Table 8.5: All identified transitions for the sources G31.41+0.31 and W3(H_2O), with integrated peak area listed.

Species	Freq (MHz)	E_{up} (K)	A (s^{-1})	Transition	G31.41+0.31 (K kms^{-1})	W3(H_2O) (K kms^{-1})
CH_3OCHO	228628.876	118.8	1.66E-04	$18_{5132} \rightarrow 17_{5122}$	-	0.39
CH_3OCHO	228651.404	118.8	1.66E-04	$18_{5130} \rightarrow 17_{5120}$	-	0.53
CH_3COCH_3	228668.358	85.4	1.69E-04	$14_{961} \rightarrow 13_{852}$	-	0.24
CH_3OCHO	229388.947	217.0	1.62E-05	$23_{9150} \rightarrow 23_{8160}$	0.79	-
CH_3OCHO	229405.021	110.7	1.75E-04	$18_{3152} \rightarrow 17_{3142}$	2.18	0.78
CH_3OCHO	229420.342	110.7	1.75E-04	$18_{3150} \rightarrow 23_{3140}$	1.86	0.71
CH_3OCHO	229504.724	134.3	1.18E-05	$20_{3170} \rightarrow 19_{4160}$	1.52	-
CH_3OH	229589.056	374.4	2.08E-05	$15_{40} \rightarrow 16_{30}$	2.58	1.06
CH_3OH	229758.756	89.1	4.19E-05	$8_{10} \rightarrow 7_{00}$	7.17	-
CH_3OCHO	236355.948	128.0	1.93E-04	$20_{3181} \rightarrow 19_{3171}$	2.38	-
CH_3OCHO	236365.574	128.0	1.93E-04	$20_{3180} \rightarrow 19_{3170}$	1.93	-
CH_3NH_2	236408.788	60.8	5.94E-05	$6_{21} \rightarrow 6_{10}$	0.44	-
HCCCN	236512.777	153.2	1.05E-03	$26 \rightarrow 25$	4.67	2.27
H_2CS	236726.770	58.6	1.91E-04	$7_{17} \rightarrow 6_{16}$	7.54	5.75
CH_3OCHO	236743.697	129.6	1.86E-04	$19_{5151} \rightarrow 18_{5141}$	2.21	?[a]
CH_3OCHO	236759.687	129.6	1.86E-04	$19_{5150} \rightarrow 18_{5140}$	1.40	0.53
CH_3OCHO	236800.589	136.7	1.80E-04	$19_{6141} \rightarrow 18_{6131}$	1.21	?
CH_3OCHO	236810.314	136.7	1.81E-04	$19_{6140} \rightarrow 18_{6130}$	2.50	1.20
CH_3OH	236936.089	260.2	2.79E-05	$14_{10} \rightarrow 13_{20}$	2.74	1.91
CH_3OCHO	236975.844	320.3	2.01E-04	$22_{1224} \rightarrow 21_{1214}$	0.86	0.33
CH_3OCHO	236976.390	320.3	2.01E-04	$22_{0225} \rightarrow 21_{0210}$	0.86	0.33
CH_3OCHO	236975.844	320.3	2.01E-04	$22_{1224} \rightarrow 21_{1214}$	1.19	0.52
CH_3OCHO	236976.390	320.3	2.01E-04	$22_{0225} \rightarrow 21_{0215}$	1.19	0.52
CH_3OCH_3	237046.092	31.3	2.33E-05	$7_{253} \rightarrow 6_{163}$	2.90	0.80
CH_3OCH_3	237046.106	31.3	2.33E-05	$7_{252} \rightarrow 6_{162}$	2.90	0.80
CH_3OCH_3	237048.797	31.3	2.32E-05	$7_{251} \rightarrow 6_{161}$	2.90	0.80
CH_3OCH_3	237051.495	31.3	2.33E-05	$7_{250} \rightarrow 6_{160}$	2.90	0.80
SO_2	237068.870	94.0	1.14E-04	$12_{39} \rightarrow 12_{210}$	1.07	1.96
$OC^{34}S$	237273.635	119.6	3.88E-05	$20 \rightarrow 19$	1.24	0.58
CH_3OCHO	237297.482	128.0	1.95E-04	$20_{2182} \rightarrow 19_{2172}$	?	2.45
CH_3OCHO	237309.540	131.6	1.98E-04	$21_{2201} \rightarrow 20_{2191}$	?	2.45
CH_3OCHO	237315.082	131.6	1.98E-04	$21_{2200} \rightarrow 20_{2190}$	?	2.45
CH_3OCHO	237344.870	131.6	1.98E-04	$21_{1202} \rightarrow 20_{1192}$	3.48	1.19
CH_3OCHO	237350.386	131.6	1.98E-04	$21_{1200} \rightarrow 20_{1190}$	3.48	1.19
OCS	243218.040	122.6	4.18E-05	$20 \rightarrow 19$	-	2.95
CH_3OCH_3	259982.561	226.6	7.27E-05	$20_{5162} \rightarrow 20_{4172}$	-	1.54
CH_3OCH_3	259982.596	226.6	7.27E-05	$20_{5163} \rightarrow 20_{4173}$	-	1.54
CH_3OCH_3	259984.480	226.6	7.27E-05	$20_{5161} \rightarrow 20_{4171}$	-	1.54
CH_3OCH_3	259982.561	226.6	7.27E-05	$20_{5160} \rightarrow 20_{4170}$	-	1.54
NH_2CHO	260189.848	92.4	1.25E-03	$12_{210} \rightarrow 11_{29}$	-	1.46
$H^{13}CO+$	260255.339	25.0	1.33E-03	$3 \rightarrow 2$	-	11.76
CH_3OCH_3	260327.165	208.3	7.21E-05	$19_{5152} \rightarrow 19_{4162}$	-	1.27
CH_3OCH_3	260327.238	208.3	7.21E-05	$19_{5153} \rightarrow 19_{4163}$	-	1.27
CH_3OCH_3	260329.312	208.3	7.21E-05	$19_{5151} \rightarrow 19_{4161}$	-	1.27
CH_3OCH_3	260331.422	208.3	7.21E-05	$19_{5150} \rightarrow 19_{4160}$	-	1.27
SiO	260518.020	43.8	7.21E-05	$6 \rightarrow 5$	-	9.24

Notes. [a] Indicates an identified transition where it was not possible to determine the peak area.

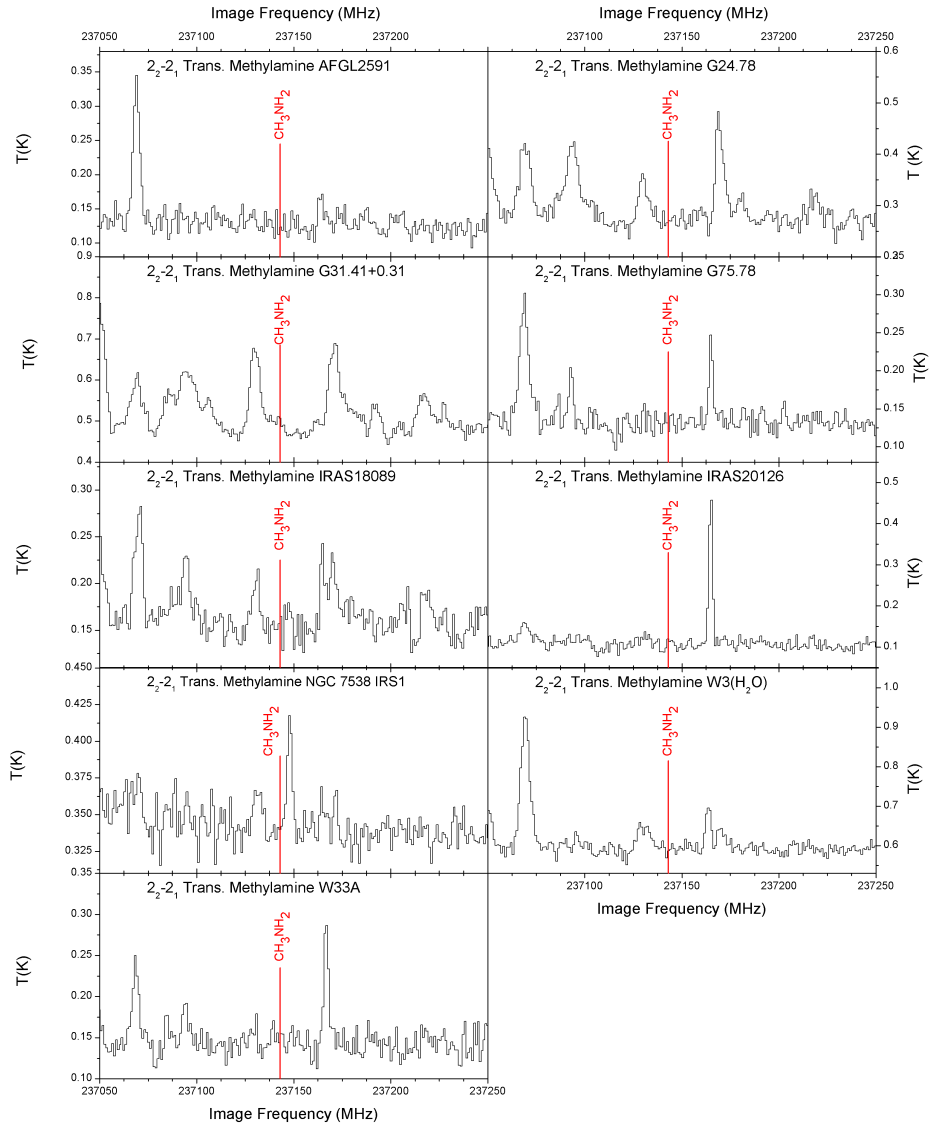

Figure 8.4: Blow-up of the spectral region around the $2_2 \rightarrow 2_1$ transition at 237143 MHz of all analysed hot cores. Despite being a particularly strong transition, it was not observed in any of the spectra.

8.7.2. ALMA

In the following figure the simulated spectrum of methylamine is shown for a column density of 1.0×10^{15} cm^{-2} at an excitation temperature of 120 K. Simulations were done with CASSIS using the JPL spectroscopic database. The frequency ranges were taken to cover ALMA Bands 6 and 7. The resolution was set at 0.1 MHz for this spectrum.

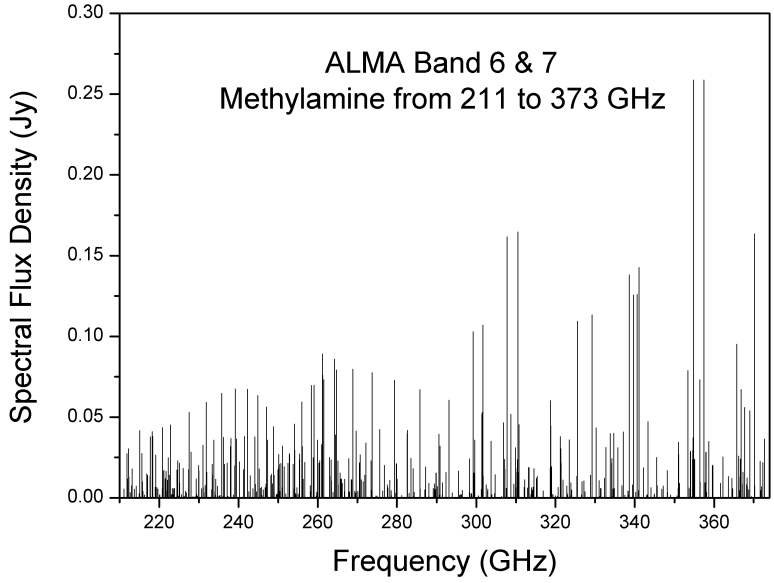

Figure 8.5: 211 to 373 GHz spectrum of methylamine, covering ALMA bands 6 and 7. A column density of 10^{15} cm^{-2}, T_{rot} and beam size of 1″ are used.

Table 8.6: Methylamine transition target candidates for ALMA Band 6 and 7

Transition	Freq (MHz)	E_{up} (K)	A (s^{-1})
$7_{2\,6} \rightarrow 7_{1\,6}$	227498.06	75.4	4.80E-05
$5_{2\,6} \rightarrow 5_{1\,6}$	232003.95	47.7	4.73E-05
$8_{2\,3} \rightarrow 8_{1\,2}$	235735.04	92.8	6.13E-05
$7_{2\,2} \rightarrow 7_{1\,3}$	239209.63	75.8	6.29E-05
$6_{2\,3} \rightarrow 6_{1\,2}$	242262.02	60.9	6.39E-05
$5_{2\,2} \rightarrow 5_{1\,3}$	244886.90	48.1	6.42E-05
$8_{0\,5} \rightarrow 7_{1\,5}$	259042.46	77.0	5.73E-05
$6_{2\,2} \rightarrow 6_{1\,3}$	261252.89	60.9	7.14E-05
$8_{0\,2} \rightarrow 7_{1\,3}$	261563.15	76.8	5.98E-05
$4_{1\,5} \rightarrow 3_{0\,5}$	264172.21	25.9	8.74E-05
$8_{2\,2} \rightarrow 8_{1\,3}$	268898.14	92.8	7.44E-05
$9_{0\,5} \rightarrow 8_{1\,5}$	299189.80	96.1	8.78E-05
$9_{0\,3} \rightarrow 8_{1\,2}$	301654091	95.9	9.11E-05
$5_{-1\,3} \rightarrow 4_{0\,2}$	307791.75	36.3	1.44E-04
$14_{2\,2} \rightarrow 14_{-1\,3}$	310750.84	240.0	8.33E-05
$10_{0\,5} \rightarrow 9_{1\,5}$	338628.32	117.3	1.25E-04
$10_{0\,2} \rightarrow 9_{-1\,3}$	341059.48	117.1	1.30E-04
$6_{1\,2} \rightarrow 5_{0\,3}$	354843.73	49.2	2.16E-04
$6_{1\,5} \rightarrow 5_{0\,5}$	357440.12	49.5	2.16E-04
$3_{2\,4} \rightarrow 2_{1\,4}$	370166.34	28.4	2.11E-04